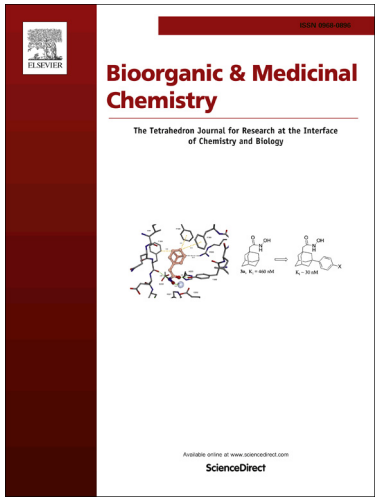

Synthesis, kinetic mechanism and docking studies of vanillin derivatives as inhibitors of mushroom tyrosinase

Zaman Ashraf, Muhammad Rafiq, Sung-Yum Seo, Mustafeez Mujtaba Babar, Najam-us-Sahar Sadaf Zaidi

PII: S0968-0896(15)00562-3
DOI: http://dx.doi.org/10.1016/j.bmc.2015.06.068
Reference: BMC 12424

To appear in: *Bioorganic & Medicinal Chemistry*

Received Date: 6 May 2015
Revised Date: 26 June 2015
Accepted Date: 27 June 2015

Please cite this article as: Ashraf, Z., Rafiq, M., Seo, S-Y., Babar, M.M., Zaidi, N.S., Synthesis, kinetic mechanism and docking studies of vanillin derivatives as inhibitors of mushroom tyrosinase, *Bioorganic & Medicinal Chemistry* (2015), doi: http://dx.doi.org/10.1016/j.bmc.2015.06.068

Synthesis, kinetic mechanism and docking studies of vanillin derivatives as inhibitors of mushroom tyrosinase

Zaman Ashraf[1,2], Muhammad Rafiq[1], Sung-Yum Seo[1,*], Mustafeez Mujtaba Babar[3], Najam-us-Sahar Sadaf Zaidi[3]

[1]*Department of Biology, College of Natural Sciences, Kongju National University, Gongju 314-701, Republic of Korea*

[2]*Department of Chemistry, Allama Iqbal Open University, Islamabad 44000, Pakistan*

[3]*Atta-ur-Rahman School of Applied Biosciences, National University of Sciences and Technology, H-12, Kashmir Highway, Islamabad, 44000, Pakistan*

Keywords: Vanillin derivatives; Synthesis; Mushroom Tyrosinase Inhibitors; Kinetic Mechanism, In silico docking

To whom correspondence should be addressed:

Sung-Yum Seo,

Tel.: 0082-41-850-8503; Fax: 0082-41-854-8503;

Email: dnalove@kongju.ac.kr

Abstract

The purpose of the present study was to discover the extent of contribution to antityrosinase activity by adding hydroxy substituted benzoic acid, cinnamic acid and piperazine residues to vanillin. The study showed the transformation of vanillin into esters as shown in **(4a-4d)**, **(6a-6b)**, and **(8a-8b)**. In addition, the relationship between structures of these esters and their mushroom tyrosinase inhibitory activity was explored. The kinetics of inhibition on mushroom tyrosinase by these esters was also investigated. It was found that hydroxyl substituted benzoic acid derivatives were weak inhibitors; however hydroxy or chloro substituted cinnamic acid and piperazine substituted derivatives were able to induce significant tyrosinase inhibition. The mushroom tyrosinase (PDBID 2ZWE) was docked with synthesized vanillin derivatives and their calculated binding energies were compared with experimental IC_{50} values which provided positive correlation. The most potent derivative 2-(4-formyl-2-methoxyphenoxy)-2-oxoethyl (2E)-3-(4-hydroxyphenyl)prop-2-enoate **(6a)** possesses hydroxy substituted cinnamic acid scaffold having IC_{50} value 16.13 µM with binding energy of -7.2 Kcal/mol. The tyrosinase inhibitory activity of **(6a)** is comparable with standard kojic acid. Kinetic analysis indicated that compound 6a was mixed-type tyrosinase inhibitor with inhibition constant values *Ki* (13 µM) and *Ki'* (53 µM) and formed reversible enzyme inhibitor complex. The active vanillin analogue **(6a)** was devoid of toxic effects as shown in cytotoxic studies.

Introduction

Tyrosinase (EC 1.14.18.1), a membrane bound copper-containing glycoprotein, regulates the biosynthesis of melanin in melanocytic cells. In mammals L-tyrosine is oxidized by tyrosinase to dopaquinone through L-3,4-dihydorxyphenylalanine (L-DOPA). Dopaquinone is then transformed through several reactions into brown to black melanin. Melanin determines the color of human skin, hair, and eyes. The actual color of skin is determined by the type and amount of melanin and its distribution pattern in the surrounding keratinocytes.[1] There are certain other environmental, hormonal and genetic factors such as UV exposure, α-melanocyte-stimulating hormone, melanocortin 1 receptor, and agouti-related protein which are involved in regulation of melanogenesis.[2,3] Melasma and post-inflammatory hyperpigmentation (PIH) are the most common pigmentation disorders for which patients seek treatment.[4] The melanocyte disorders such as senile lentigo, freckles and pigmented acne scars occur in human of all races worldwide.[5] Such disorders may have major influence on a person's psychological and social well-being resulting in lower output, overall functioning, and self-confidence.[6]

Tyrosinase is also responsible for the production of neuromelanins but excessive production of dopaquinones by oxidation of dopamine results in neuronal damage and cell death. This links tyrosinase to Parkinson's and other neurodegenerative diseases.[7-9] It has also been reported that tyrosinase is one of the main causes of most fruit and vegetable damage during postharvest handling and processing, leading to quicker degradation and lesser shelf life.[10-12] A number of researchers reviewed the importance of mushroom tyrosinase, defined its biochemical characteristics and inhibition as well as activation by several inhibitors from natural and synthetic origin for their use in food and cosmetic industry.[13-16] Tyrosinase is also linked to the sclerotization of cuticle, defensive encapsulation and melanization of foreign organism and wound healing in insects.[17] These biochemical processes offer probable targets for the development of safer and effective tyrosinase inhibitors as insecticides and eventually for insect control. Thus, the development of safe and effective tyrosinase inhibitors is of great concern in the medical, agricultural and cosmetic industries.

The pharmacophore modeling and molecular docking has recently developed as a powerful method complementing traditional high through put screenings. Molecular docking is an optimization problem that would define the "best-fit" positioning of a compound that binds to a

specific protein of interest.[18-19] The computational chemistry and chemoinformatics play an important role in preliminary drug research.

A number of aromatic aldehydes possessing electron donating or electron withdrawing groups at 3 or 4 position of benzene ring have been reported for their potential for inhibition of tyrosinase.[20-23] Nihei and coworkers reported that 2-hydroxy-4-isopropyl benzaldehyde, known as chamaecin, showed potent tyrosinase inhibition activity with IC_{50} 2.3 μM.[24] Vanillin (4-hydroxy-3-methoxybenzaldehyde) is a well-known natural product and is extensively used as flavoring agent in food and cosmetics with an estimated yearly universal consumption of synthetic vanillin more than 200 tons. Additionally, vanillin displays antimicrobial, anticancer and antioxidant activities. Also, it has been used as a potential starting material for the production of fine chemicals cationic surfactants.[25-26] It was also reported that vanillin and vanillic acid isolated from *Origanum vulgare* may serve as agents for antimelanogenesis.[27] Most of the clinically used tyrosinase inhibitors such as kojic acid, arbutine, oxyresveratrol, *p*-coumaric acid, kaempferol, glabridin etc., all possess free phenolic hydroxyl moiety which play important role in tyrosinase inhibitory activity.[28-29] The presence of these structural features may help in the designing of more potent tyrosinase inhibitors. Hence, vanillin was selected as a core structure for the concise and cost-effective synthesis of ester derivatives having hydroxy substituted aryl moiety for their improved tyrosinase inhibitory activity. Vanillin derivatives have also been synthesized by incorporating heterocyclic piperazine ring to explore its role in tyrosinase inhibitory activity.

Material and Methods

All chemicals used for the synthesis of compounds were purchased from Sigma Chemical Co. Melting points were determined using a Digimelt MPA 160, USA melting point apparatus and are reported uncorrected. The FT-IR spectra were recorded with Shimadzu FTIR–8400S spectrometer (Kyoto, Japan, υ, cm^{-1}). The ^{1}H NMR and ^{13}C NMR spectra ($CDCl_3$) and (DMSO-d_6) were recorded using a Bruker 400 MHz spectrometer. Chemical shifts (δ) are reported in ppm downfield from the internal standard tetramethylsilane (TMS). The purity of the compounds was checked by thin layer chromatography (TLC) on silica gel plate using n-hexane and ethyl acetate as mobile phase. The procedure for the synthesis of the desired compounds is depicted in Scheme I, II and III.

Reagents

Mushroom tyrosinase was purchased from Sigma (USA); L-DOPA and vanillin were purchased from Sigma (USA). Stock solutions of the reducing substrates were prepared in phosphate buffer (20 mM, pH 6.8).

Synthesis of vanillin chloroacetyl derivative (2)

A mixture of vanillin **(1)** (0.01 mol), triethylamine (0.01 mol) in anhydrous dichloromethane (25 mL) was cooled in an ice salt mixture to 0 to -5 ^{o}C. To this reaction mixture, chloroacetyl chloride (0.01 mol) in dry dichloromethane was added drop wise with constant stirring over a period of 1 h maintaining the temperature constant. The reaction mixture was then stirred at room temperature for further 5h, washed with 5 % HCl, and 5 % sodium hydroxide solution. The organic layer was washed with saturated aqueous NaCl, dried over anhydrous magnesium sulphate, filtered and solvent was removed under reduced pressure. The crude product was purified by silica gel column to afford the corresponding vanillin chloroacetyl derivative **(2)** as white solid.

4-formyl-2-methoxyphenyl chloroacetate **(2)** White solid; reaction time, 5 h; yield, 82 %; melting point, 63-65 °C; R_f 0.64 (n-hexane:ethyl acetate 2:1), FTIR ν_{max} cm^{-1}: 3016 (sp2 C-H), 2960 (sp3 C-H), 1761 (C=O ester), 1689 (C=O Aldehyde), 1598 (C=C aromatic); **^{1}H NMR (DMSO-d_6, δ ppm)**: 9.99 (s, 1H, CHO), 7.65 (d, *J*=1.6 Hz, 1H, H-2), 7.62 (dd, *J*=6.4, 2.0 Hz, 1H, H-6), 7.43 (d, *J*=8.0 Hz, 1H, H-5), 4.76 (s, 2H, -CH_2), 3.89 (s, 3H, -OCH_3); **^{13}C NMR (DMSO-d_6, δ ppm)**; 192.5 (C=O, Aldehyde), 165.8 (C=O ester), 151.8 (C-3), 144.0 (C-4), 135.9 (C-1), 124.0 (C-5), 123.9 (C-6), 112.7 (C-2), 59.8 (OCH_3), 56.0 (CH_2).

Synthesis of vanillin analogues (4a-4d) and (6a-6b)

A mixture of vanillin chloroacetyl derivative **(2)** (0.01 mol), hydroxy substituted benzoic acids **(3a-g)** (0.01mole), triethyl amine (0.01 mol), potassium iodide (0.01 mol) in dimethyl formamide (25 mL) was stirred overnight at room temperature **(Scheme I)**. The reaction mixture was poured into finely crushed ice with stirring and extracted with ethyl acetate (4x25 mL). The combined organic layer was washed with 5 % HCl, 5 % sodium hydroxide and finally with aqueous NaCl solution. The organic layer was dried over anhydrous magnesium sulphate, filtered and the solvent was removed under reduced pressure to afford the crude products **(4a-d)**.

The title compounds **(4a-d)** were purified by silica gel column chromatography. The same procedure was used for the preparation of compounds **(6a** and **6b) Scheme II**.

2-(4-formyl-2-methoxyphenoxy)-2-oxoethyl 4-hydroxybenzoate **(4a)** solid; reaction time, 24 h; yield, 76 %; melting point, 111-113 °C; R_f 0.46 (n-hexane:ethyl acetate 2:1),FTIR ν_{max} cm^{-1}: 3126 (O-H), 2940 (sp2 C-H), 2820(sp3 C-H), 1723 (C=O ester), 1690 (C=O Aldehyde), 1588 (C=C aromatic), 1143 (C-O, ester); **^{1}H NMR (DMSO-d_6, δ ppm)**: 9.78 (s, 1H, -CHO), 8.12 (d, *J*=8.0 Hz, 1H, H-6'), 7.90 (dd, *J*=6.8, 2.0 Hz, 2H, H-2, H-6), 7.64 (dd, *J*=6.6, 2.0 Hz, 1H, H-5'), 7.59 (d, *J*=2.0 Hz, 1H, H-3'), 6.89 (dd, *J*=5.2, 2.8 Hz, 2H, H-3, H-5), 5.20 (s, 2H, -CH_2), 3.88 (s, 3H, -OCH_3), 2.50 (s, 1H, -OH); **^{13}C NMR (DMSO-d_6, δ ppm)**; 191.4 (C=O Aldehyde), 166.2 (C=O Aliphatic ester), 164.8 (C=O Aromatic ester), 163.0 (C-4), 153.5 (C-1'), 148.6 (C-2'), 135.8 (C-4'), 132.3 (C-2, C-6), 129.1 (C-1), 123.9 (C-5'), 122.5 (C-6'), 119.5 (C-3'), 115.8 (C-3, C-5), 60.9 (CH_2), 56.6 (-OCH_3).

2-(4-formyl-2-methoxyphenoxy)-2-oxoethyl 2,4-dihydroxybenzoate **(4b)** solid; reaction time, 24 h; yield, 70 %; melting point, 141-143 °C; R_f 0.42 (n-hexane:ethyl acetate 2:1), FTIR ν_{max} cm^{-1}: 3320 (O-H), 2943 (sp2 C-H), 2867 (sp3 C-H), 1741 (C=O ester), 1687 (C=O Aldehyde), 1604 (C=C aromatic), 1123 (C-O, ester); **^{1}H NMR (DMSO-d_6, δ ppm)**: 9.77 (s, 1H, -CHO), 7.73 (d, *J*=8.8 Hz, 1H, H-6), 7.64 (d, *J*=1.6 Hz, 1H, H-3'), 7.61 (dd, *J*=6.0, 2.0 Hz, 1H, H-5'), 7.43 (d, *J*=4.4, 1H, H-6'), 6.43 (dd, *J*=6.4, 2.4 Hz, 1H, H-5), 6.35 (d, *J*=2.4 Hz, 1H, H-3), 5.28 (s, 2H, -CH_2), 3.88 (s, 3H, -OCH_3), 3.36 (s, 2H, -OH); **^{13}C NMR (DMSO-d_6, δ ppm)**; 192.4 (C=O Aldehyde), 168.3 (C=O Aliphatic ester), 166.2 (C=O Aromatic ester), 165.1 (C-2), 163.2 (C-4), 151.8 (C-1'), 143.7 (C-2'), 135.8 (C-4'), 132.6 (C-6), 129.1 (C-3'), 124.1 (C-5'), 112.7 (C-6'), 110.9 (C-5), 109.1 (C-3), 103.9 (C-1), 61.4 (CH_2), 56.5 (-OCH_3).

2-(4-formyl-2-methoxyphenoxy)-2-oxoethyl 3,4-dihydroxybenzoate **(4c)** solid; reaction time, 24 h; yield, 76 %; melting point, 144-145 °C; R_f 0.40 (n-hexane:ethyl acetate 2:1), FTIR ν_{max} cm^{-1}: 3290 (O-H), 2976 (sp2 C-H), 2856 (sp3 C-H), 1726 (C=O ester), 1692 (C=O Aldehyde), 1594 (C=C aromatic), 1178 (C-O, ester); **^{1}H NMR (DMSO-d_6, δ ppm)**: 9.78 (s, 1H, -CHO), 7.75 (d, *J*=8.8 Hz, 1H, H-6'), 7.64 (d, *J*=1.2 Hz, 1H, H-3'), 7.62 (dd, *J*=6.4, 1.2 Hz, 1H, H-5'), 7.42 (d, *J*=8.0 Hz, 1H, H-5), 6.43 (dd, *J*=6.4, 2.4 Hz, 1H, H-6), 6.34 (d, *J*=2.4 Hz, 1H, H-2), 5.24 (s, 2H, -CH_2), 3.88(s, 3H, -OCH_3), 3.35 (s, 2H, -OH); **^{13}C NMR (DMSO-d_6, δ ppm)**;192.5 (C=O Aldehyde), 168.2 (C=O Aliphatic ester), 166.2 (C=O Aromatic ester), 165.1 (C-4), 163.2 (C-3),

151.8 (C-1'), 143.7 (C-2'), 135.8 (C-4'), 132.5 (C-6), 124.0 (C-3'), 115.1 (C-5'), 112.7 (C-6'), 109.1 (C-2), 103.9 (C-5), 103.1 (C-1), 61.1 (CH_2), 56.5 (-OCH_3).

2-(4-formyl-2-methoxyphenoxy)-2-oxoethyl 3,5-dihydroxybenzoate **(4d)** solid; reaction time, 24 h; yield, 81 %; melting point, 138-139 °C; R_f 0.38 (n-hexane:ethyl acetate 2:1), FTIR ν_{max} cm^{-1}: 3354 (O-H), 2971 (sp2 C-H), 2887 (sp3 C-H), 1735 (C=O ester), 1676 (C=O Aldehyde), 1601 (C=C aromatic), 1154 (C-O, ester); **^{1}H NMR (DMSO-d_6, δ ppm)**: 9.78 (s, 1H, -CHO), 7.43 (dd, *J*=6.4, 1.6 Hz, 1H, H-5'), 7.39 (d, *J*=2.0 Hz, 1H, H-3'), 6.96 (d, *J*=8.0 Hz, 1H, H-6'), 6.89 (dd, *J*=2.4, 2.4 Hz, 2H, H-2, H-6), 6.50 (dd, *J*=2.4, 2.4 Hz, 1H, H-4), 4.87 (s, 2H, -CH_2), 3.71 (s, 3H, -OCH_3), 3.32 (s, 2H, -OH); **^{13}C NMR (DMSO-d_6, δ ppm)**; 191.4 (C=O Aldehyde), 168.5 (C=O Aliphatic ester), 167.1 (C=O Aromatic ester), 159.1 (C-3, C-5), 153.5 (C-1'), 148.6 (C-2'), 130.8 (C-4'), 129.1 (C-2, C-6), 126.5 (C-3'), 115.8 (C-5'), 111.1 (C-6'), 108.2 (C-1), 107.7 (C-4), 61.5 (CH_2), 56.0 (-OCH_3).

2-(4-formyl-2-methoxyphenoxy)-2-oxoethyl (2E)-3-(4-hydroxyphenyl)prop-2-enoate **(6a)** solid; reaction time, 24 h; yield, 72 %; melting point, 145-147 °C; R_f 0.48 (n-hexane:ethyl acetate 2:1), FTIR ν_{max} cm^{-1}: 3410 (O-H), 2939 (sp2 C-H), 2851 (sp3 C-H), 1715 (C=O ester), 1702 (C=O ester), 1680 (C=O aldehyde), 1600 (C=C aliphatic) 1588 (C=C aromatic), 1167 (C-O, ester); **^{1}H NMR (DMSO-d_6, δ ppm)**: 9.77 (s, 1H, -CHO), 7.87 (d, *J*=8.8 Hz, 1H, H-6''), 7.82 (d, *J*=16.0 Hz, 1H, H-3), 7.64 (dd, *J*=6.8, 1.6 Hz, 2H, H-2', H-6'), 7.42 (dd, *J*=8.0, 1.6 Hz, 1H, H-5''), 7.25 (dd, *J*=9.4, 1.6 Hz, 2H, H-3', 5'), 6.76 (d, *J*=2.0 Hz, 1H, H-3''), 6.55 (d, *J*=16.0 Hz, 1H, H-2), 5.15 (s,2H, -CH_2), 3.89 (s, 3H, -OCH_3), 1.99 (s, 1H, -OH); **^{13}C NMR (DMSO-d_6, δ ppm)**; 192.5 (C=O Aldehyde), 166.3 (C=O ester), 165.9 (C=O ester), 160.5 (C-4'), 151.8 (C-2''), 146.8 (C-3), 145.4 (C-4''), 135.8 (C-1'), 132.3 (C-1''), 131.1 (C-2',6'), 130.5 (C-3',5'), 125.3 (C-2), 124.0 (C-3''), 116.2 (C-5''), 113.2 (C-6''), 60.9 (-OCH_3), 56.6 (-CH_2).

2-(4-formyl-2-methoxyphenoxy)-2-oxoethyl (2E)-3-(4-chlorophenyl)prop-2-enoate **(6b)** solid; reaction time, 24 h; yield, 88 %; melting point, 134-136 °C; R_f 0.51 (n-hexane:ethyl acetate 2:1), FTIR ν_{max} cm^{-1}: 3018 (sp2 C-H), 2940 (sp3 C-H), 1780 (C=O ester), 1723 (C=O), 1690 (C=O aldehyde), 1602 (C=C aliphatic), 1588 (C=C aromatic), 1108 (C-O, ester); **^{1}H NMR (DMSO-d_6, δ ppm)**: 9.98 (s, 1H, -CHO), 7.84 (dd, *J*=9.6, 1.6 Hz, 2H, H-2',6'), 7.81 (d, *J*=2.0 Hz, 1H, H-3''), 7.80 (d, *J*=16.4 Hz, 1H, H-3), 7.64 (dd, *J*=3.6, 2.0 Hz, 1H, H-5''),7.52 (dd, *J*=9.2, 1.6 Hz, 2H, H-3', 5'), 7.42 (d, *J*=8.0 Hz, 1H, H-6''), 6.79 (d, *J*=16.0 Hz, 1H, H-2), 5.15 (s,2H, -CH_2),

3.89 (s, 3H, -OCH_3); **^{13}C NMR (DMSO-d_6, δ ppm)**;192.4 (-CHO), 166.3 (C=O ester), 165.9 (C=O, ester),151.8 (C-2''), 145.1 (C-3), 143.8 (C-4''), 135.8 (C-1'), 134.9 (C-1''), 133.2 (C-2',6'), 130.9 (C-4'), 130.8 (C-3',5'), 129.4 (C-2), 123.9 (C-3''), 118.0 (C-5''), 112.7 (C-6''), 60.9 (-OCH_3), 56.6 (-CH_2).

Synthesis of vanillin analogues (8a-8b)

A solution of N-substituted piperazines **(7a-7b)** (0.01mol) and vanillin chloroacetyl derivative **(2)** (0.011mol) in anhydrous dichloromethane (25 mL) was mixed with triethyl amine (0.03mol) at ambient temperature. The mixture was stirred for two days, then CH_2Cl_2 (50 mL) was added. The products were sequentially washed with saturated Na_2CO_3 (30 mL x 2), with saturated sodium chloride and dried over anhydrous magnesium sulphate **(Scheme III)**. After filtration and removal of the solvent under reduced pressure, the crude products were purified by silica gel column chromatography to afford the title compounds **(8a-8b)**.

4-formyl-2-methoxyphenyl (4-methylpiperazin-1-yl)acetate **(8a)** solid; reaction time, 24h; yield, 81 %; melting point, 66-68 °C; R_f 0.58 (n-hexane:ethyl acetate 2:1), FTIR ν_{max} cm^{-1}: 2987 (sp2 C-H), 2820 (sp3 C-H), 1725 (C=O ester), 1656 (C=O Aldehyde), 1597 (C=C aromatic), 1348 (C-N); **^{1}H NMR (DMSO-d_6, δ ppm)**: 9.84 (s, 1H, -CHO), 7.33 (d, *J*=2.0 Hz, 1H, H-3'), 7.29 (dd, *J*=5.2, 2.0 Hz, 1H, H-5'), 6.96 (d, *J*=6.4 Hz, 1H, H-6'), 4.92 (s, 2H -CH_2), 4.15 (s, 3H, -OCH_3), 3.70 (m, 4H, H-3, H-5), 3.20 (m, 4H, H-2, H-6), 1.27 (s, 3H, -CH_3); **^{13}C NMR (DMSO-d_6, δ ppm)**; 190.8 (-CHO), 164.2 (C=O ester), 140.2 (C-2'), 138.2 (C-1'), 122.3 (C-5'), 115.4 (C-3'), 114.4 (C-4'), 108.8 (C-6'), 56.1 (-OCH_3), 43.2 (CH_2), 31.9 (C-2, C-6), 29.6 (C-3, C-5), 14.1 (CH_3).

4-formyl-2-methoxyphenyl (4-phenylpiperazin-1-yl)acetate **(8b)** solid; reaction time, 24 h; yield, 84 %; melting point, 70-72 °C; R_f 0.52 (n-hexane:ethyl acetate 2:1), FTIR ν_{max} cm^{-1}: 2967 (sp2 C-H), 2865 (sp3 C-H), 1743 (C=O ester), 1687 (C=O Aldehyde), 1590 (C=C aromatic), 1365 (C-N); **^{1}H NMR (DMSO-d_6, δ ppm)**: 9.84 (s, 1H, -CHO), 7.33 (dd, *J*=5.2, 2.0 Hz, 1H, H-5'), 7.29 (d, *J*=2.0 Hz, 1H, H-3'), 6.96 (d, *J*=6.4 Hz, 1H, H-6'), 6.92-6.94 (m, 5H, 4-phenyl), 4.92 (s, 2H -CH_2), 4.13 (s, 3H, -OCH_3), 3.69 (m, 4H, H-3, H-5), 3.23 (m, 4H, H-2, H-6); **^{13}C NMR (DMSO-d_6, δ ppm)**; 192.4 (-CHO), 165.1 (C=O ester), 150.9 (C-2''), 150.7 (C-1''), 149.1

(C-1'), 129.3 (C-3', C-5'), 120.7 (C-2', C-6'), 117.1 (C-4'), 116.8 (C-5''), 114.4 (C-3''), 112.5 (C-4''), 108.8 (C-6''), 56.0 (-OCH_3), 49.9 (C-2, C-6), 49.2 (C-3, C-5), 46.2 (CH_2).

Mushroom tyrosinase inhibition assay

The mushroom tyrosinase (EC 1.14.18.1) (Sigma Chemical Co.) was used for in vitro bioassays as described previously with some modifications.[30-31] Briefly, 140 µL of phosphate buffer (20 mM, pH 6.8), 20 µL of mushroom tyrosinase (30 U/mL) and 20 µL of the inhibitor solution were placed in the wells of a 96-well micro plate. After pre-incubation for 10 min at room temperature, 20 µL of L-DOPA (3,4-dihydroxyphenylalanine) (0.85 mM) was added and the plate was further incubated at 25 °C for 20 min. Subsequently the absorbance of dopachrome was measured at 475 nm using a micro plate reader (OPTI $_{Max}$, Tunable). Kojic acid was used as a reference inhibitor and phosphate buffer was used instead of the inhibitor solution for negative control. The extent of inhibition by the test compounds was expressed as the percentage of concentration necessary to achieve 50 % inhibition (IC_{50}). Each concentration was analyzed in three independent experiments. The IC_{50} values were determined by the data analysis and graphing software Origin 8.6, 64-bit.

Free radical scavenging assay

Radical scavenging activity was determined by modifying already reported method[32-33] by 2,2-diphenyl-1-picrylhydrazyl (DPPH) assay. The assay solution consisted of 100 µL of DPPH (150 µM), 20 µL of increasing concentration of test compounds and the volume was adjusted to 200 µL in each well with DMSO. The reaction mixture was then incubated for 30 minutes at room temperature. Ascorbic acid (Vitamin C) was used as a reference inhibitor. The assay measurements were carried out by using a micro plate reader ($OPTI_{Max}$, Tunable) at 517 nm. The reaction rates were compared and the percent inhibition caused by the presence of tested inhibitors was calculated. Each concentration was analyzed in three independent experiments run in triplicate.

Kinetic analysis of the inhibition of tyrosinase

A series of experiments were performed to determine the inhibition kinetics of derivatives **4b**, **6a**, **6b**, and **8a** by following the already reported method.[34-35] The inhibitor concentrations are: 0, 72.2, 144.5 and 289 µM for **4b**; 0, 8.75 and 17.5 µM for **6a**; 0, 8.3, 16.6 and 33.3 µM for

6b; 0, 10.68, 21.37, 42.75, 85.5 and 342 µM for **8a**. Substrate L-DOPA concentration was between 0.0625 to 2 mM in all kinetic studies. Pre-incubation and measurement time was the same as discussed in mushroom tyrosinase inhibition assay protocol. Maximal initial velocity was determined from initial linear portion of absorbance up to five minutes after addition of enzyme at a 15s interval. The inhibition type on the enzyme was assayed by Lineweaver–Burk plots of inverse of velocities (1/*V*) versus inverse of substrate concentration 1/[S] mM^{-1}. The EI dissociation constant *Ki* was determined by secondary plot of 1/*V* versus inhibitors concentrations while ESI dissociation constant *Ki'* was determined by intercept versus inhibitors concentrations. The reversible kinetics of the enzyme inhibitor complex was also determined for different concentration of derivatives **6a** and **8a** versus the enzyme concentration (4, 6, 8, 10, 15 and 20 µg/mL).

Molecular Modeling

Protein preparation and Grid Selection

Molecular docking analysis of the synthesized compounds was performed to determine the relative affinity with tyrosinase enzyme using the AutoDock Vina (1.1.2).[36] The program helps in determining the binding affinity of the ligand molecules with the tertiary structure of the protein. Moreover, by default 9 different binding conformations are generated for each molecular docking analysis. For the analysis, the tertiary structure of tyrosinase was retrieved from the RCSB Protein Databank using the PDBID 2ZWE.[37-38] The tertiary structure is based on sequence homology modeling. The model contains a complex of two proteins; tyrosinase enzyme and a caddie protein melC/ORF378. Moreover, copper ions, nitrate ions and solvent molecules have also been represented in the crystal structure. In order to modify the protein for docking analysis, Discovery Studio (4.1.0) was used.[39] The caddie protein, bound to the active site of the tyrosinase, was removed. Moreover, the solvent molecules and nitrate ions were also removed. The active site of the molecule comprises the amino acid residues surrounding the two copper ions. After modifying the enzyme and confirming that there were no chemical entities that could hinder the ligand-protein binding, the protein structure was saved in pdb format. Using AutoDock Tools (1.5.6), the crystal structure was then prepared for docking. For the purpose, the molecule was protonated and energy was minimized. Moreover, the search space coordinates for the binding of the ligand to the protein molecule were also defined. The search space grid box

was set in a manner that it ensured that the active site was fully enclosed. Therefore, the spacing was kept at 1Å with 40x40x40 as the size for x, y and z coordinates. The center of x, y and z axes were kept at -11,-13 and 12. Default values were retained for the rest of the parameters. The protein was then saved in pdbqt format that could be read by AutoDock Vina for determining binding potential of the ligands with the molecule.

Ligand preparation

The ligand molecules were sketched in ChemSketch software (11.02) and subjected to 3-D auto-optimization. The structures were saved in mol format and the files were converted to pdb format using ArgusLab (v.4.0.1).[40] The files were retrieved in the AutoDock Tools to determine and optimize the ligand geometry and bond flexibility based upon semi-empirical method. The ligand structures were then saved in pdbqt format.

Docking analysis and visualization

After the protein and ligand files had been prepared, docking analysis was performed using AutoDock Vina. The program employs an iterated local search algorithm using the user-provided search parameters. The docking for each ligand was carried out 10 times on 3 different computer platforms in order to remove machine based bias. Output was obtained in the form of binding energy (kcal/mol) and binding pose file for each ligand-protein binding conformation. The best ligand binding pose was selected on the basis of binding energy, number and nature of amino acid residues involved in the interaction, type of interaction and intermolecular distance between the ligand atoms and the amino acid residues. The selected pose was visualized in Discovery Studio. Both 2-D and 3-D ligand interaction maps were generated in order to determine the amino acids involved in binding of the ligand to the crystal structure of the protein.

Cell viability assay

The cell viability experiment using 3-(4,5-Dimethylthiazol-2-yl)-2,5-diphenyltetrazolium Bromide (MTT) assay was performed to investigate cytotoxicity of compound **6a.** The mouse skin fibroblast (L929) and human keratinocyte (HaCaT) were cultured in 48 well plates (Crystal grade polystyrene, gamma sterilized, SPL Korea) using complete DMEM medium containing 1 % antibiotics and 10 % fetal bovine serum. The cells ($5x10^4$ cells/well) were incubated 24 hours before exposing to the various concentrations of test compound. The vanillin analogue **6a** was

dissolved in DMSO and diluted with DMEM medium to achieve final concentrations; 0, 8.70, 17.4 and 35.1µM. Then cells in the presence of compound **6a** were again incubated for 24 hours at 37 °C and 5 % CO_2. Then MTT assay was conducted, absorbance was measured at 570 nm by using ELISA reader and all determinations were performed in triplicate. All data were expressed as a mean ± standard deviation and significance was analyzed using Student's t-tests. Statistical significance was considered as ($p<0.005$).

Results and discussion

Synthesis

The vanillin derivatives **(4a-4d)**, **(6a-6b)**, and **(8a-8b)** were synthesized by following the already reported method[41] with some modification shown in **Scheme I**, **II** and **III**. The vanillin chlroacetyl derivative **(2)** was synthesized by esterification of phenolic -OH group of vanillin with chloroacetyl chloride in the presence of $(C_2H_5)_3N$ and anhydrous methylene chloride as solvent. The presence of a singlet at 4.76ppm for methylene protons in ^{1}HNMR and a signal at 56.0ppm for methylene carbon in ^{13}CNMR spectra confirm the formation of precursor **(2)**. The final products **(4a-4d)** and **(6a-6b)** were prepared by simple nucleophilic substitution at **(2)** with hydroxy substituted benzoic acids **(3a-3d)** and para substituted cinnamic acids **(5a-5b)** respectively. The title compounds **(8a-8b)** were prepared by incorporation of the N-methyl and N-phenyl substituted piperazine moiety. All of the synthesized compounds have been characterized by FTIR, ^{1}H NMR and ^{13}C NMR spectroscopic data.

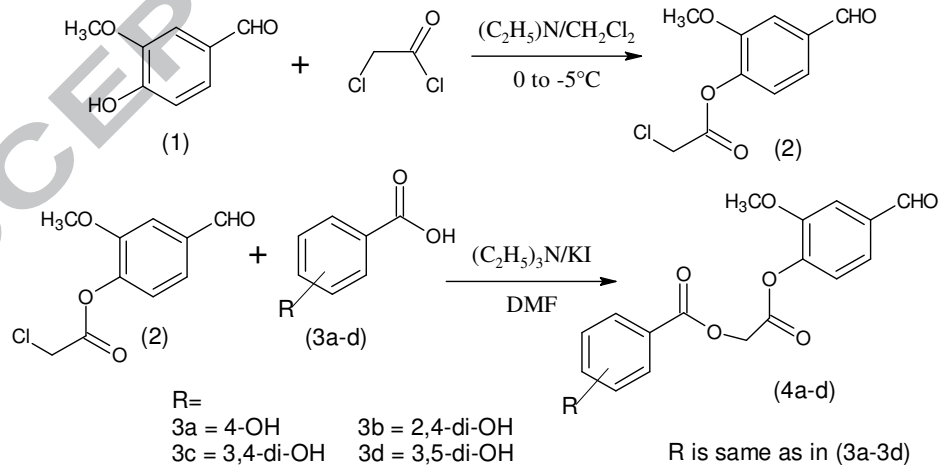

Scheme I Synthesis of vanillin analogues **(4a-4d)**

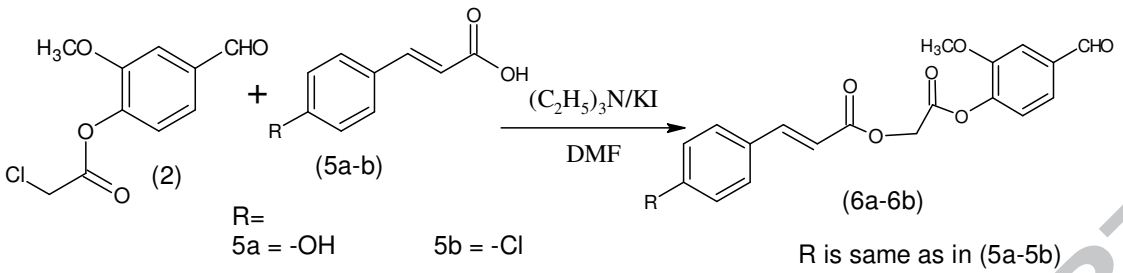

Scheme II Synthesis of vanillin analogues **(6a-6b)**

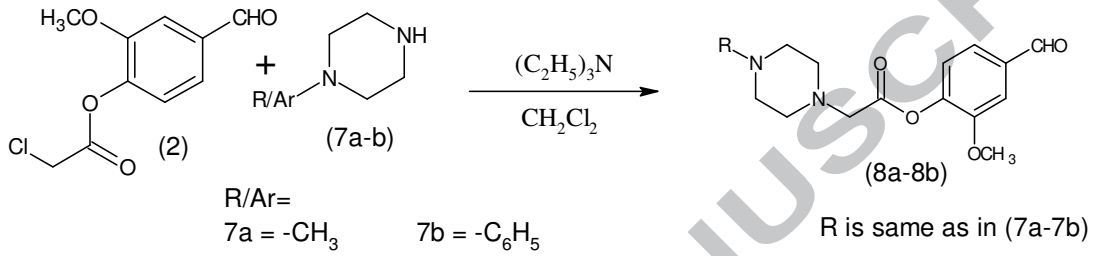

Scheme III Synthesis of vanillin analogues **(8a-8b)**

Bioassay for tyrosinase inhibitory activity

Inhibitory effects of the synthesized vanillin derivatives on mushroom tyrosinase activity have been evaluated. Kojic acid, a competitive tyrosinase inhibitor, was used as standard in this study for comparison purposes. The synthesized compounds **4b**, **6a**, **6b**, and **8a** showed good to excellent inhibition of mushroom tyrosinase with IC_{50} ranged from 16.13 µM to 42.60 µM while rest of the vanillin analogues displayed lesser activities compared to standard kojic acid. Table 1 presented the IC_{50} values of the synthesized vanillin derivatives and it was observed that compound **6a** exhibited the most potent tyrosinase inhibitory activity with IC_{50} 16.13 µM. The presence of the hydroxy substituted cinnamic acid moiety in compound **6a** plays very important role in the tyrosinase inhibitory activity as it showed same enzyme inhibition response at a lower dose than the standard kojic acid. The role of chlorine in tyrosinase inhibitory activity was also investigated in case of compound **6b**. The derivative **6b** possesses chlorine at position 4 of the phenyl ring of cinnamic acid having IC_{50} 30.85 µM and showed activity lower than compound **6a.** It showed higher activity than derivatives with mono- and dihydroxy substituted benzoic acids scaffold. The compound **4b** possesses a 2,4-dihydroxy substituted benzoic acid moiety and exhibited higher tyrosinase inhibition potential with IC_{50} 42.60 µM than the derivatives which

possess mono substituted or 3,4-dihydroxy or 3,5-dihydroxy substituted benzoic acid functionality. The compound **8a** showed excellent tyrosinase inhibitory activity with IC_{50} 21.60 µM more active than all other derivatives except compound **6a**. It possesses N-methyl substituted piperazine ring which plays vital role in inhibition of tyrosinase activity. The IC_{50} value of vanillin reported in literature[19] is 70.0 mM; all of the reported vanillin analogues have higher potential to inhibit the activity of tyrosinase than vanillin. It is worth noting that antityrosinase activity was increased when chloroacetyl vanillin derivative **2** was esterified with hydroxy substituted cinnamic acid rather than monohydroxy or dihydroxy substituted benzoic acids. On the basis of the results we propose that vanillin derivative **6a** may serve as a structural model for the design and development of novel tyrosinase inhibitors.

Table 1 The inhibitory effects of vanillin derivatives on mushroom tyrosinase activity: (substrate: L-DOPA).

Compounds	Tyrosinase Activity IC_{50} ± SEM[a] µM	DPPH Assay % Inhibition ± SEM (100 µg/mL)[b]
2	78.9 ± 5.87	18 ± 1
4a	201.15 ± 21.9	10 ± 1
4b	42.60 ± 14.5	13 ± 2
4c	156.87 ± 25.1	17 ± 1
4d	59.76 ± 2.02	16 ± 2
6a	16.13 ± 0.94	1 ± 1
6b	30.85 ± 11.8	7 ± 1
8a	21.60 ± 2.43	1 ± 1
8b	101.38 ± 18.5	4 ± 1
Kojic acid	16.69 ± 2.8	---
Vitamin C	---	97 ± 1

[a]SEM=Standard error of the mean; values are expressed in mean ± SEM for three parallel measurements
[b]All inhibitors and vitamin C concentrations are 100 µg/mL

Kinetic Mechanism

Based upon our results we selected the most potent vanillin derivatives **4b**, **6a**, **6b** and **8a** to determine their inhibition type and inhibition constants on mushroom tyrosinase activity. The potential of these derivatives to inhibit the free enzyme and enzyme-substrate complex was determined in terms of EI and ESI constants respectively. The kinetic studies of the enzyme by the Lineweaver–Burk plot of 1/*V* versus 1/[S] in the presence of different inhibitors concentrations gave a series of straight lines as shown in **Fig 1-4(a)**. The results of **Fig 1-3(a)** showed that compounds **4b**, **6a**, and **6b** intersected within the second quadrant. The analysis

showed that V_{max} decreased with increasing K_m in the presence of increasing concentrations of compounds **4b**, **6a**, and **6b**, respectively. This behavior of vanillin derivatives **4b, 6a,** and **6b** indicated that it inhibits tyrosinase by two different pathways[42]; competitively forming enzyme-inhibitor (EI) complex and interrupting enzyme-substrate-inhibitor (ESI) complex in non-competitive manner. The secondary plots of slope versus concentration of compounds **4b**, **6a**, and **6b** showed EI dissociation constants *Ki* **Fig. 1-3(b)**, while ESI dissociation constants *Ki'* were shown by secondary plots of intercept versus concentration of compounds **4b**, **6a**, and **6b**, **Fig. 1-3(c)**. A lower value of *Ki* than *Ki'* pointed out stronger binding between enzyme and compounds **4b**, **6a** and **6b** which suggested preferred competitive over noncompetitive manners (Table 2). While in case of compound **8a**, Lineweaver–Burk plot gave family of straight lines, all of which intersected at the same point on the x-axis **Fig. 4(a)**.The analysis showed that $1/V_{max}$ increased to a new value while that of K_m remains the same as a result of increase in the concentrations of compound **8a**. This behavior indicated that compound **8a** inhibits tyrosinase non-competitively to form enzyme inhibitor (EI) complex.[33] Secondary plot of slope against concentration of **8a** showed EI dissociation constant (*Ki*) **Fig. 4(b)**. The results of kinetic constants and inhibition constants are summarized in Table 2.

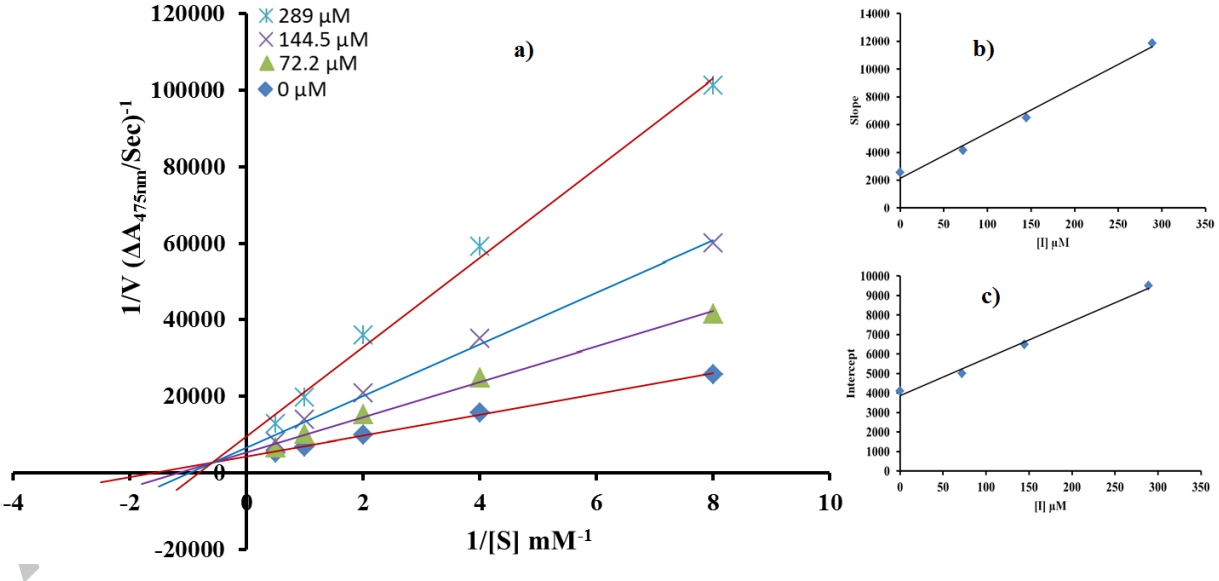

FIGURE 1 Lineweaver–Burk plots for inhibition of tyrosinase in the presence of Compound **4b**. (**a**) Concentrations of **4b** were 0, 72.2, 144.5 and 289 µM, respectively. Substrate L-DOPA Concentrations were 0.125, 0.25, 0.5, 1 and 2 mM, respectively. (**b**) The insets represent the plot of the slope or (**c**) of the vertical intercepts versus inhibitor **4b** concentrations to determine inhibition constants. The lines were drawn using linear least squares fit.

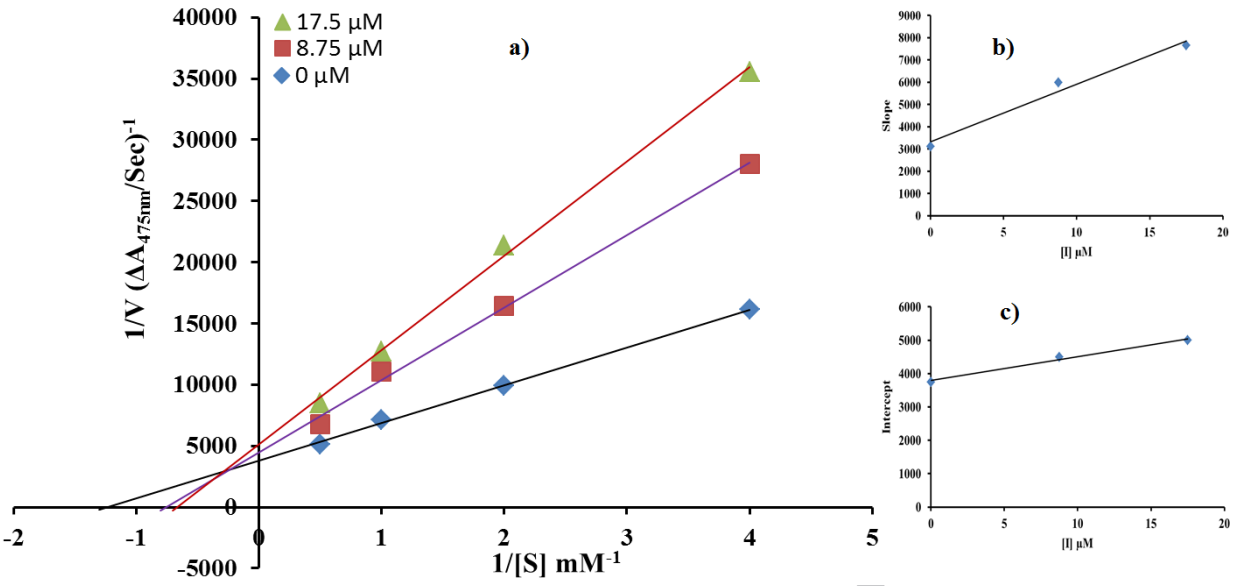

FIGURE 2 Lineweaver–Burk plots for inhibition of tyrosinase in the presence of Compound **6a**. (**a**) Concentrations of **6a** were 0, 8.75 and 17.5 µM, respectively. Substrate L-DOPA Concentrations were 0.25, 0.5, 1 and 2 mM, respectively. (**b**) The insets represent the plot of the slope or (**c**) the vertical intercepts versus inhibitor **6a** concentrations to determine inhibition constants. The lines were drawn using linear least squares fit.

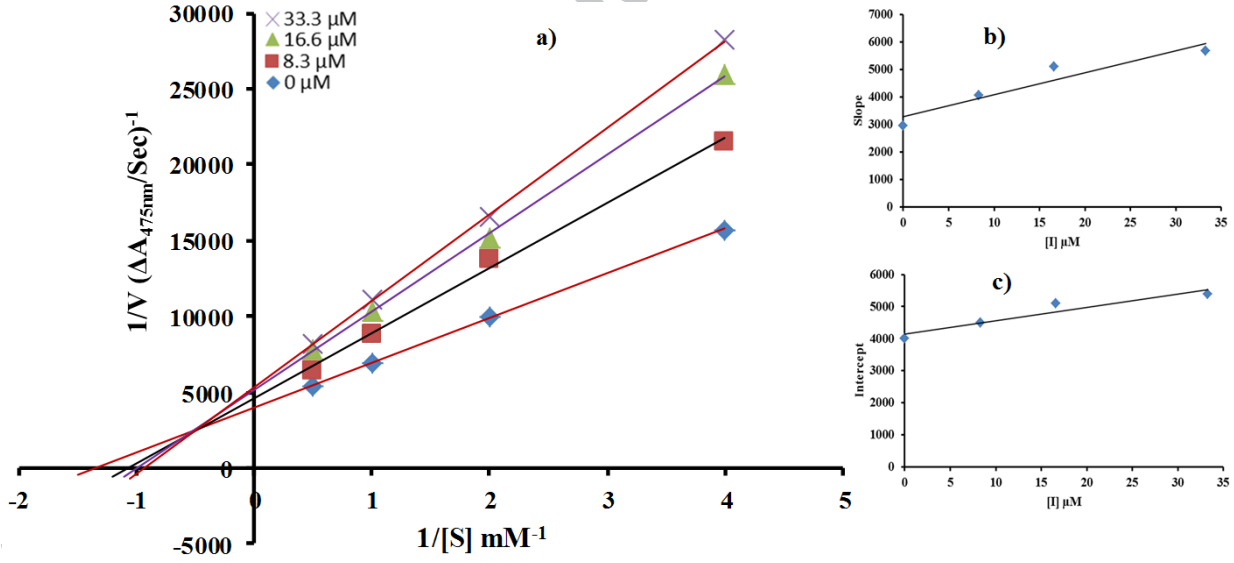

FIGURE 3 Lineweaver–Burk plots for inhibition of tyrosinase in the presence of Compound **6b**. (**a**) Concentrations of **6b** were 0, 8.3, 16.6 and 33.3 µM, respectively. Substrate L-DOPA Concentrations were 0.25, 0.5, 1 and 2 mM, respectively. (**b**) The insets represent the plot of the slope or (**c**) of the vertical intercepts versus inhibitor **6b** concentrations to determine inhibition constants. The lines were drawn using linear least squares fit.

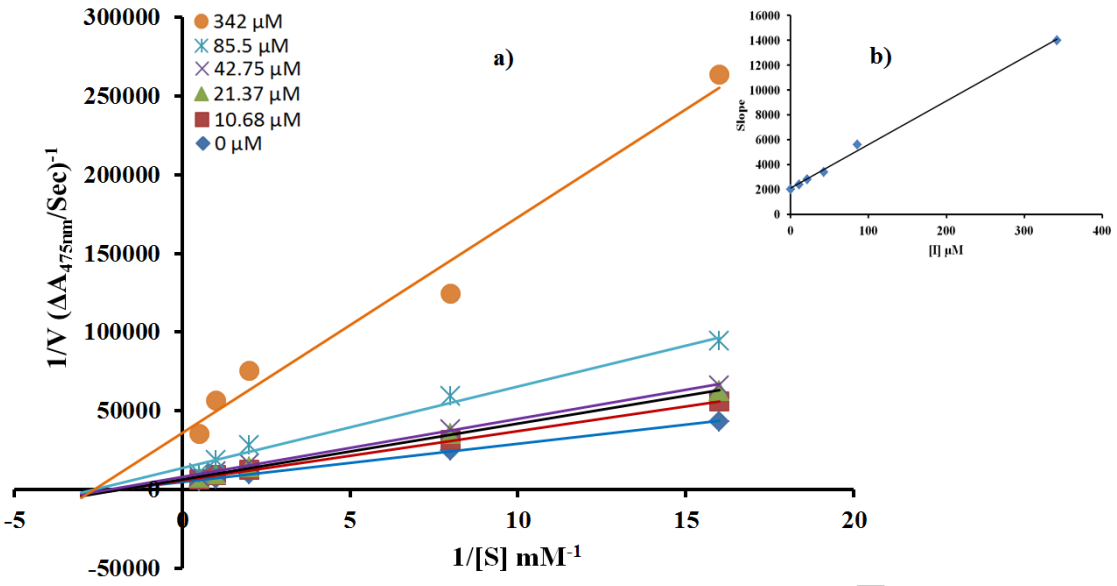

FIGURE 4 Lineweaver–Burk plots for inhibition of tyrosinase in the presence of Compound **8a**. (**a**) Concentrations of **8a** were 0, 10.68, 21.37, 42.75, 85.5 and 342 µM, respectively. Substrate L-DOPA Concentrations were 0.062, 0.125, 0.5, 1 and 2 mM, respectively. (**b**) The insets represent the plot of the slope versus inhibitor (8a) concentrations to determine inhibition constant. The lines were drawn using linear least squares fit.

Table 2 Kinetic parameters of the mushroom tyrosinase for L-DOPA activity in the presence of different concentration of vanillin derivatives **4b**, **6a**, **6b** and **8a**.

Code	Dose (µM)	V_{max} (ΔA /Sec)	K_m (mM)	Inhibition Type	Inhibition	*Ki* (µM)	*Ki'* (µM)
	0	2.44×10^{-4}	0.62				
4b	72.2	2.00×10^{-4}	0.83	Mixed-inhibition	---	65	205
	144.5	1.53×10^{-4}	1.00				
	289.0	1.05×10^{-4}	1.25				
	0	2.66×10^{-4}	0.83				
6a	8.75	2.22×10^{-4}	1.33	Mixed-inhibition	Reversible	13	53
	17.5	2.00×10^{-4}	1.53				
	0	2.50×10^{-4}	0.74				
6b	8.3	2.22×10^{-4}	0.90	Mixed-inhibition	---	41	100
	16.6	1.96×10^{-4}	1.00				
	33.3	1.85×10^{-4}	1.05				
	0	2.0×10^{-4}	0.4				
	10.68	1.66×10^{-4}	0.4				
8a	21.37	1.42×10^{-4}	0.4	Non-competitive	Reversible	60	---
	42.75	1.17×10^{-4}	0.4				
	85.5	7.14×10^{-5}	0.4				
	342	2.85×10^{-5}	0.4				

V_{max} is the reaction velocity

K_m is the Michaelis-Menten constant

Ki is the EI dissociation constant

Ki' is the ESI dissociation constant

--- Not determined

The reversibility of the enzyme inhibitor complex was also studied for compounds **6a** and **8a**. **Fig. 5** and **Fig. 6** showed the remaining enzyme activity versus the concentration of enzyme (4, 6, 8, 10, 15 and 20 µg/mL) in the presence of different concentrations of compounds **6a** and **8a** for the catalysis of L-DOPA respectively. Increasing the inhibitor concentration resulted in a decrease in the slope of the lines, which indicate that the enzyme undergoes a reversible inhibition.

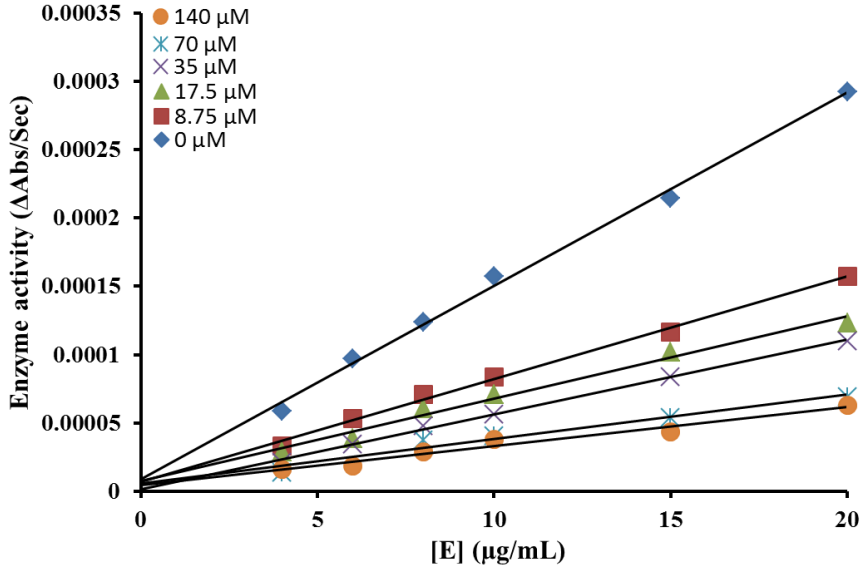

FIGURE 5 Effects of concentrations of mushroom tyrosinase on its activity for the catalysis of L-DOPA at different concentrations of inhibitor **6a**.

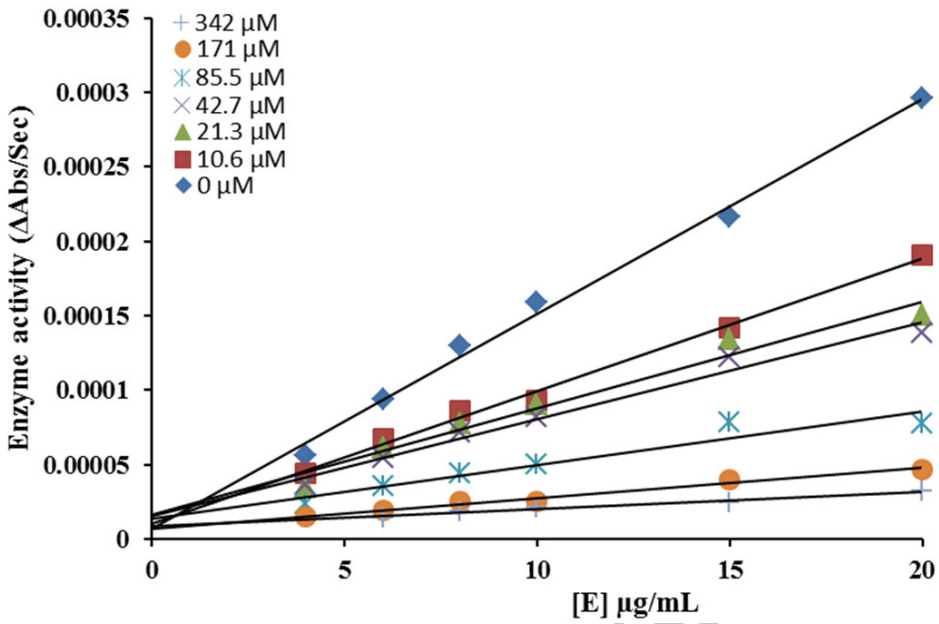

FIGURE 6 Effects of concentrations of mushroom tyrosinase on its activity for the catalysis of L-DOPA at different concentrations of inhibitor **8a**.

DPPH radical scavenging assay

All of the synthesized vanillin derivatives were evaluated for the DPPH free radical scavenging ability. The synthesized compounds showed no radical scavenging potential even at high concentration (100µg/mL).

Docking studies

In an attempt to theoretically describe the difference found in the antityrosinase activity of the synthesized vanillin derivatives, docking studies using tyrosinase enzyme (2ZWE) were performed. The molecular construction and the docking analysis were accomplished as described in the subsequent section. All of the computationally predicted lowest energy complexes are stabilized by the intermolecular hydrogen bonds and stacking interactions. The steric bulk and type of functional groups determine the interactions in these complexes. The binding affinities of the enzyme-inhibitor complexes during docking were calculated and presented in Table 3. The lower value showed the more stable complex formed between the ligand and target protein. The vanillin derivative **6a** showed the lowest binding energy calculated during docking studies (-7.2 kcal/mol), whereas the binding energies of compounds **4b**, **6b** and **8a** were -7.0, -6.7, -6.5 kcal/mol, respectively. The values of binding energies proved that compound **6a** formed the most

stable drug receptor complex with target protein. The possible enzyme-inhibitor interactions of derivatives **4b**, **6a**, **6b** and **8a** with the active site of mushroom tyrosinase are shown in **Fig.7 to Fig.10**, respectively.

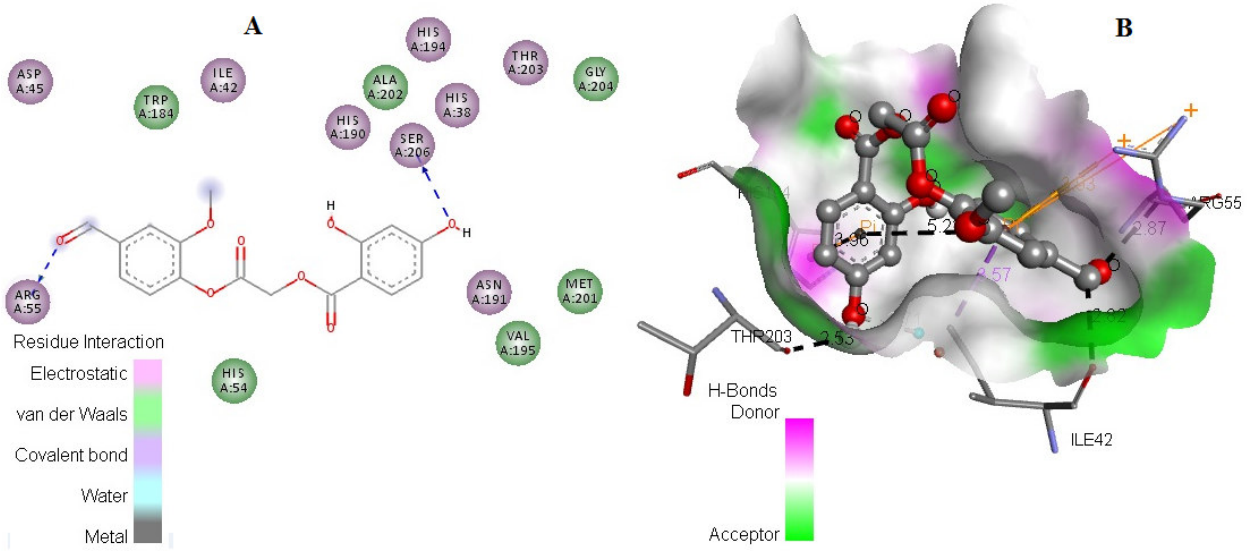

FIGURE 7 The ligand-protein interactions of compound **4b** with the active site of mushroom tyrosinase (2ZWE) generated by using Discovery Studio 4.0. The (A) shows the two dimensional interaction patterns. The legend inset represents the type of interaction between the ligand atoms and the amino acid residues of the protein. The (B) shows the three-dimensional docking of the compound in the binding pocket. Dashed lines indicate the interactions between the ligand and the amino acids of the receptor.

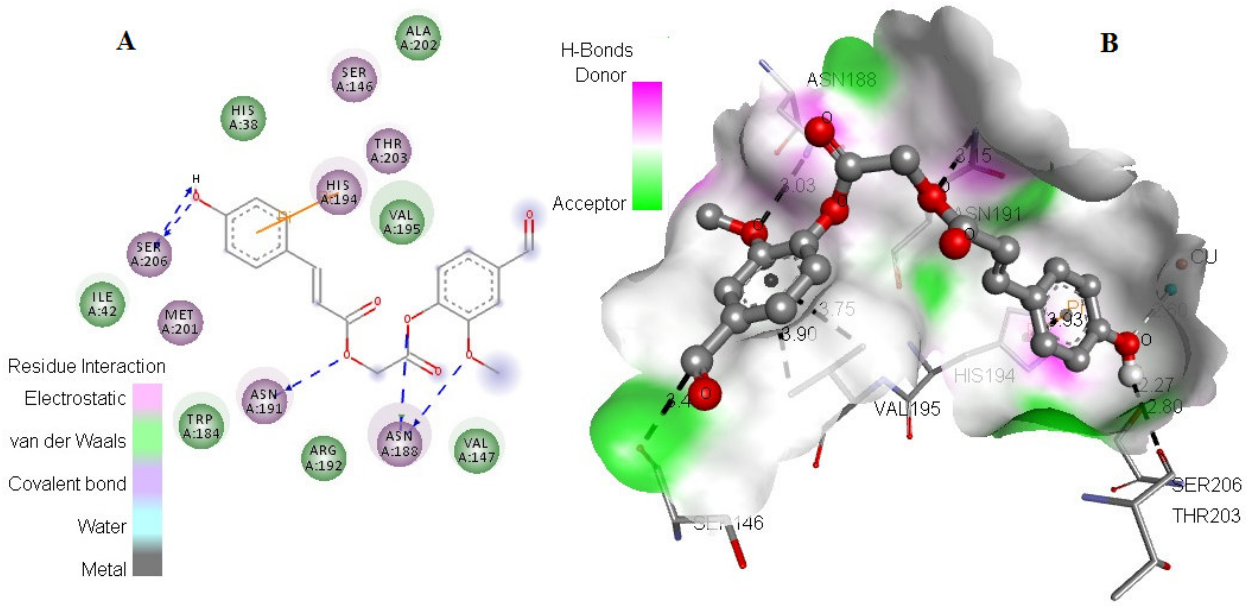

FIGURE 8 The ligand-protein interactions of compound **6a** with the active site of mushroom tyrosinase (2ZWE) generated by using Discovery Studio 4.0. The (A) shows the two dimensional interaction patterns. The legend inset represents the type of interaction between the ligand atoms and the amino acid residues of the protein. The (B) shows the three-dimensional docking of the compound in the binding pocket. Dashed lines indicate the interactions between the ligand and the amino acids of the receptor.

Table 3 The average binding energy was calculated after docking of synthesized vanillin derivatives

Compounds	Average Binding Energy kcal/mol	Log*P*[a]
4a	-6.7	2.89± 0.37
4b	-6.9	2.94±0.41
4c	-7.0	2.62± 0.41
4d	-6.5	2.72± 0.41
6a	-7.2	2.66± 0.40
6b	-6.7	3.73±0.40
8a	-6.5	0.75±0.45
8b	-5.7	3.04± 0.50

[a]Log*P* calculated from ChemSketch ACD labs 2012

There is a hydrogen bond between phenolic hydroxyl in case of compound **6a** and amino acid SER206 of the enzyme with bond length 2.27Å (**Fig. 8**). The methoxy of vanillin ring in the same compound formed a hydrogen bond with ASN188 having bond distance 3.03Å and ester oxygen is linked with ASN191 with bond length 3.15Å of the target enzyme. There is also π-π stacking present between cinnamic acid phenyl ring and HIS194 residue of the tyrosinase having bond distance 3.93Å. **Figure 7** depicted different types of interactions present between

compound **4b** and amino acid residues of the target enzyme. The aldehyde group in compound **4b** interacts with ARG55 of target protein by hydrogen bonds having bond length 2.87Å. There is also π-π stacking present between vanillin phenyl ring and ARG55 while the phenolic hydroxyl at 4-position of phenyl ring in compound **4b** forms hydrogen bond with SER206 residue of the active site of tyrosinase. For compound **6b** the carbonyl oxygen of ester functionality interacts with HIS194 through hydrogen bonding while GLY204 amino acid residue of target protein forms hydrogen bond with methoxy oxygen of vanillin ring having bond distance 3.14Å (**Fig. 9**). There are also π-π stacks interactions between phenyl ring of cinnamic acid moiety and ARG55 with bond distance 3.63Å. The aldehyde oxygen in compound **8a** interacts through hydrogen bonding with ARG55 residue of the enzyme having bond distance 3.21Å (**Fig. 10**). The calculated binding energies of derivatives **6a** and **6b** are -7.2 and -6.7 kcal/mol, respectively, the former possesses hydroxyl substituted cinnamic acid while the later has chloro substituted cinnamic acid scaffold. The docking results are in good agreement of the experimental calculated IC_{50} values. These results further confirmed that hydroxyl groups in the phenyl ring of cinnamic acid play a significant role in the formation of stable ligand-target complex as well as in mushroom tyrosinase inhibitory activity.

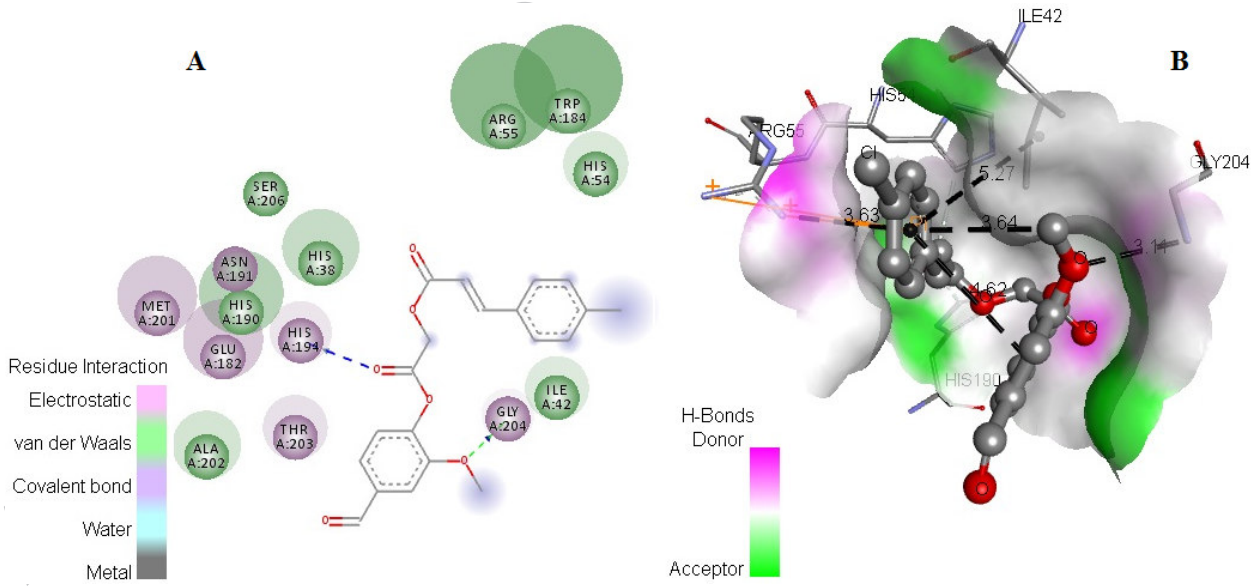

FIGURE 9 The ligand-protein interactions of compound **6b** with the active site of mushroom tyrosinase (2ZWE) generated by using Discovery Studio 4.0. The (A) shows the two dimensional interaction patterns. The legend inset represents the type of interaction between the ligand atoms and the amino acid residues of the protein. The (B) shows the three-dimensional docking of the compound in the binding pocket. Dashed lines indicate the interactions between the ligand and the amino acids of the receptor.

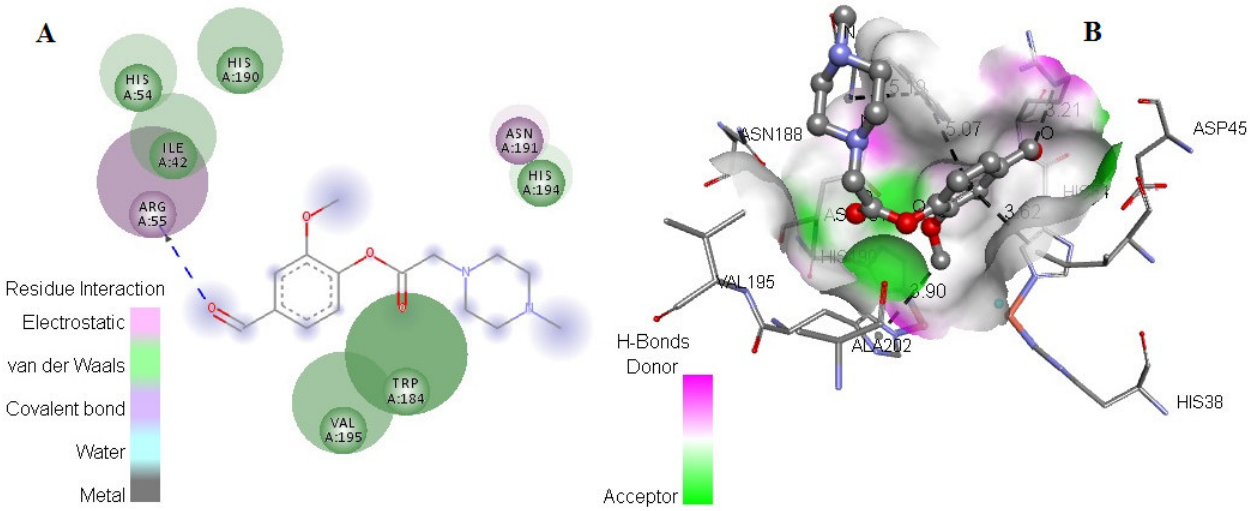

FIGURE 10 The ligand-protein interactions of compound **8a** with the active site of mushroom tyrosinase (2ZWE) generated by using Discovery Studio 4.0. The (A) shows the two dimensional interaction patterns. The legend inset represents the type of interaction between the ligand atoms and the amino acid residues of the protein. The (B) show the three-dimensional docking of the compound in the binding pocket. Dashed lines indicate the interactions between the ligand and the amino acids of the receptor.

Cytotoxicity studies

According to our results, the vanillin derivative **6a** exhibited most potent tyrosinase inhibitory activity and highest binding affinity with tyrosinase enzyme. The viability assay of derivative **6a** on mouse skin fibroblast (L929) and human keratinocyte (HaCaT) was carried out. The results showed that compound **6a** exert cytotoxic effects in a dose dependent manner **Fig. 11**. The cytotoxic effects exerted by compound **6a** are minor in case of human keratinocyte (HaCaT) at higher concentration (35.1µM). On the other hand in case of mouse skin fibroblast (L929) cytotoxic effects are smaller at lower concentration (8.7µM) and significant at higher concentration (35.1µM).

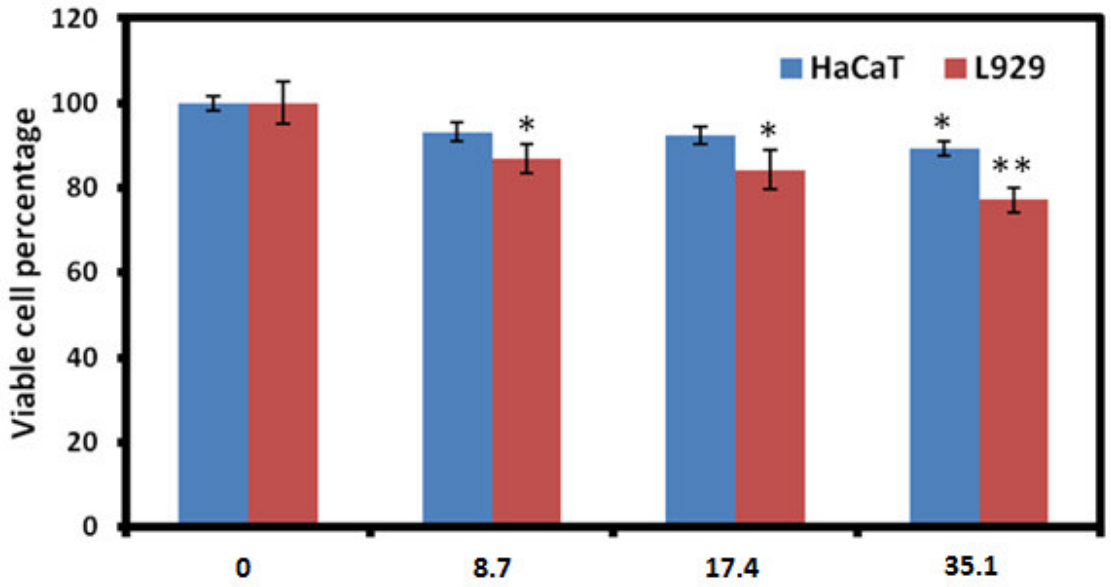

FIGURE 11 The effects of vanillin derivative **6a** on cell viability of the mouse skin fibroblast (L929) and human keratinocyte (HaCaT) cells. The cells were treated with various concentrations of compound **6a** (0, 8.70, 17.4 and 35.1 µM). All data were expressed as a mean ± standard deviation and significance was analyzed using Student's t-tests. Statistical significance was considered as $p<0.05$ (*$p<0.05$; **$p<0.005$ vs. control).

Conclusion

The vanillin derivatives with various homocyclic or heterocyclic and hydrophobic or hydrophilic moieties have been synthesized to validate their role in tyrosinase inhibitory activity. The vanillin analogue **6a** showed comparable tyrosinase inhibitory activity (IC_{50} 16.13 µM) with standard kojic acid. The kinetic analysis showed that compound **6a** was a mixed-type tyrosinase inhibitor and formed reversible enzyme inhibitor complex exhibited no cytotoxicity on mouse skin fibroblast (L929) and human keratinocyte (HaCaT) cells. The lowest energy AutoDock of the most potent analogue **6a** at the tyrosinase (2ZWE) active site revealed that hydroxy substituted cinnamic acid unit fits the enzyme-binding site well. It was confirmed that hydroxyl groups in the phenyl ring of cinnamic acid play a significant role in the formation of stable ligand-target complex as well as in mushroom tyrosinase inhibitory activity. Based on our results we propose that compound **6a** may serve as a structural model for the design and development of novel tyrosinase inhibitors.

Declaration of interest or Acknowledgement

This work (Grants No.C0036335) was supported by Business for Cooperative R & D between Industry, Academy, and Research Institute and funded by Korea Small and Medium Business Administration in 2012.

References

1. Parvez, S.; Kang, M.; Chung, H. S.; Cho, C.; Hong, M. C.; Shin, M. K.; Bae, H. *Phytother. Res.* **2006**, *20*, 921.
2. Kadekaro, A. L.; Kanto, H.; Kavanagh, R.; Abdel-Malek, Z. A. *Ann. N. Y. Acad. Sci.* **2003**, *994*, 359.
3. Petit, L.; Pierard, G. E. *Int. J. Cosmet. Sci.* **2003**, *25*, 169.
4. Lynde, C. B.; Kraft, J. N.; Lynde, C. W. *Skin Therapy Lett*. **2006**, *11*, 1.
5. Rendon, M.; Berneburg, M.; Arellano, I.; Picardo, M. *J. Am. Acad. Dermatol.* **2006**, 54 (5 Suppl 2), S272-281.
6. Finlay, A. Y. *Br. J. Dermatol*. **1997**, *136*, 305.
7. Asanuma, M.; Miyazaki, I.; Ogawa, N. *Neurotox. Res.* **2003**, *5*, 165.
8. Zhu, Y. J.; Zhou, H. T.; Hu Y. H. *Food Chem*. **2011**, *124*, 298.
9. Xu, Y.; Stokes, A. H.; Roskoski R, Jr.; Vrana, K. E. *J. Neurosci. Res.* **1998**, *54*, 691.
10. Yi, W., Cao, R. *Eur. J. Med. Chem*. **2010**, *45*, 639.
11. Friedman, M. *J. Agric. Food. Chem*. **1996**, *44*, 631.
12. Mayer, A. M. *Phytochemistry* **1987**, *26*, 11.
13. Seo, S. Y.; Sharma, V. K.; Sharma, N. *J Agric Food Chem.* **2003**, *51*, 2837.
14. Loizzo, M. R.; Tundis, R.; Menichini, F. *Compr. Rev. Food Sci. & Food Safety.* **2012**, *11*, 378.
15. Chang, T. S. *Int. J. Mol. Sci*. **2009**, *10*, 2440.
16. Khan, M. T. H. *Pure Appl. Chem*. **2007**, *79*, 2277.
17. Ashida, M.; Brey, P. *Proc. Natl. Acad. Sci. USA*. **1995**, *92*, 10698.
18. Hamed, I. A.; Keiichiro, T.; Eiichi, A.; Hiroto, K.; Shinji, M.; Hiroyuki, H.; Noriyuki, A.; Yutaka, K.; Takehiro, Y. *Bioorg. Med. Chem.,* **2007**, *15*, 242.
19. Maria, G. M.; Daniele, Z.; Luciano, V.; Maurizio, F.; Marco, F.; Sabrina, P.; Giuditta, S.; Elena, B. *Bioorg. Med. Chem.*, **2005**, *13*, 3797.
20. Kubo, I.; Kinst-Hori, I. *Planta Med*. **1999**, *65*, 19.
21. Kubo, I.; Kinst-Hori, I. *J. Agric. Food Chem*. **1998**, *46*, 5338.
22. Kubo, I.; Kinst-Hori, I. *J. Agric Food Chem*. **1999**, *47*, 4574.
23. Jimenez, M.; Chazarra, S.; Escribano, J.; Cabanes, J.; Garcia-Carmona, F. *J. Agric. Food Chem.* **2001**, *49*, 4060.
24. Nihei, K.-I.; Yamagiwa, Y.; Kamikawab, T.; Kubo, I. *Bioorg. Med. Chem. Lett.* **2004**, *14*, 681.
25. Sinha, A. K.; Sharma, U. K.; Sharma, N. *Int. J. Food Sci. Nutr*. **2008**, *9*, 299.
26. Walton, N. J.; Mayer, M. J.; Narbad, A. *Phytochemistry.* **2003**, *63*, 505.
27. Chou, T. H.; Ding, H. Y.; Hung, W. J.; Liang, C. H. *Exp. Dermatol*. **2010**, *19*, 742.

28. Neelakantan, S.; Raman, P. V.; Tinabaye, A. A. *Indian J. Chem. Sect. Bio*. **1982**, *1*, 256.
29. Rescigno, A.; Sollai, F.; Pisu, B.; Rinaldi, A.; Sanjust, E. *J. Enzyme Inhib. Med. Chem.* **2002**, *17*, 207.
30. Seo, W. D.; Ryu, Y. B.; Curtis-Long, M. J.; Lee, C. W.; Ryu, H. W.; Jang, K. C.; Park, K. H. *Eur. J. Med. Chem.* **2010**, *45*, 2010.
31. Ashraf, Z.; Rafiq, M.; Seo, S. Y.; Babar, M. M.; Zaidi, N. S. S. *J. Enzyme Inhib. Med. Chem.* **2014**, 1-10, DOI: 10.3109/14756366.2014.979346.
32. Manohara, R. S. A.; Jayesh, M.; Punit, B.; Vasanthraju, S. G.; Srinivasan, K. K.; Mallikarjuna, R. C.; Gopalan, K. N. *Bioorg. Med. Chem*. **2011**, *19*, 384.
33. Ehab, A. A.; Julie, R. M.; Ikhlas, A. K. *Bioorg. Med. Chem.* **2012**, *20*, 2784.
34. Wang, Q.; Qiu, L.; Chen, X. R.; Song, K. K.; Shi, Y.; Chen, Q. X. *Bioorg. Med. Chem.* **2007**, *15*, 1568.
35. Chiari, M. E.; Vera, D. M. A.; Palacios, S. M.; Carpinella, M. C. *Bioorg. Med. Chem.* **2011**, *19*, 3474.
36. Trott, O.; Olson. A. J. *J. comput. Chem*., **2010**, *31*, 455.
37. Matoba, Y.; Kumagai, T.; Yamamoto, A.; Yoshitsu, H.; Sugiyama, M. *J. Biol. Chem*. **2006**, *281*, 8981.
38. Berman, H. M.; Westbrook, J.; Feng, Z.; Gilliland, G.; Bhat, T.; Weissig, H.; Shindyalov, I. N.; Bourne. P. E. *The protein data bank. Nucleic Acids Res*., **2000**, *28*, 235.
39. Studio, D., **2007**. version 2.0. Accelrys Software Inc.: San Diego, CA, USA.
40. Thompson. M. Molecular docking using ArgusLab, an efficient shape-based search algorithm and the AScore scoring function, ACS meeting, Philadelphia, **2004**. p. 42.
41. Chu, W.; Tu, Z.; McElveen, E.; Xu, J.; Taylor, M.; Luedtke, R. R.; Mach, R. H. *Bioorg. Med. Chem.* **2005**, *13*, 77.
42. Rattanangkool, E.; Kittikhunnatham, P.; Damsud, T.; Wacharasindhu, S.; Phuwapraisirisan, P. *Eur. J. Med. Chem.* 2**013**, *66*, 296.

Synthesis, kinetic mechanism and docking studies of vanillin derivatives as inhibitors of mushroom tyrosinase

Graphical Abstract

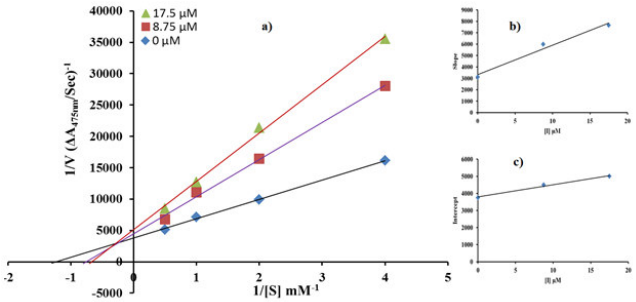

a) Lineweaver-Burk Plot
b) & c) Secondary Replots to determine *Ki* & *Ki'*

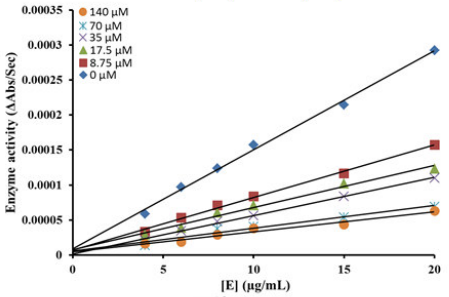

Compound Show Reversible Inhibition

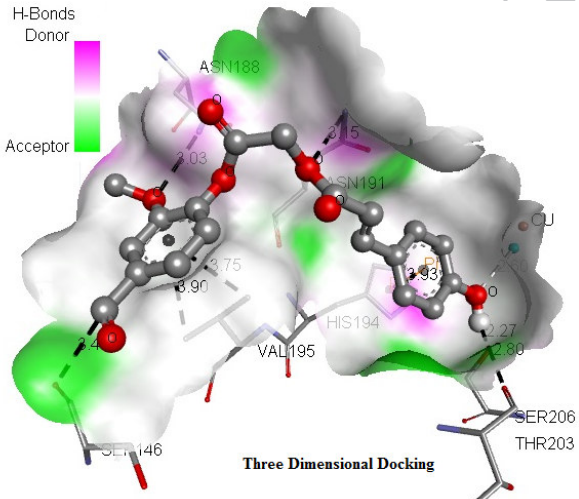

Three Dimensional Docking

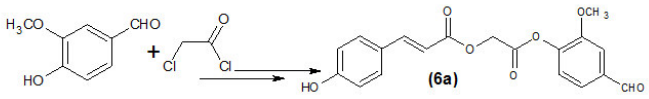

Synthetic Route